Hindawi
International Journal of Aerospace Engineering
Volume 2018, Article ID 1284753, 15 pages
https://doi.org/10.1155/2018/1284753

Research Article

Adaptive Neural Control of Hypersonic Vehicles with Actuator Constraints

Changxin Luo, Humin Lei, Dongyang Zhang, and Xiaojun Zou

Air and Missile Defence College, Air Force Engineering University, Xi'an 710051, China

Correspondence should be addressed to Changxin Luo; 1710794652@qq.com

Received 29 April 2018; Revised 17 July 2018; Accepted 26 July 2018; Published 9 September 2018

Academic Editor: Yue Wang

An adaptive neural control method is proposed in this paper for the flexible air-breathing hypersonic vehicle (AHV) with constraints on actuators. This scheme firstly converts the original control problem with input constraints into a new control problem without input constraints based on the control input saturation function. Secondly, on the basis of the implicit function theorem, the radial basis function neural network (RBFNN) is introduced to approximate the uncertain items of the model. And the minimal-learning-parameter (MLP) technique is adopted to design the adaptive law for the norm of network weight vector, which significantly reduces calculations. Meanwhile, the finite-time convergence differentiator (FD) is introduced, through which the model state variables and their derivatives are accurately estimated to ensure the control effect. Finally, it is theoretically proved that the closed-loop control system is stable. And the effectiveness of the designed controller is verified by simulation.

1. Introduction

Air-breathing hypersonic vehicle (AHV) is a new type of aircraft flying in the near space at a speed of more than Mach 5. It has outstanding advantages in terms of high speed, high maneuverability, and large flight envelope that traditional aircrafts do not have, which possesses potential applications in both civilian and military fields [1–3]. But it also has more complex coupling, stronger nonlinearity, more severe elastic vibration, and tighter control input constraints than ordinary aircraft due to the flat and slender body design of the AHV and the integration of scramjet engine, which make the flight control of AHV a frontier issue in today's control field [4, 5].

In the design process of the control law for AHV, by introducing a neural network to approximate the model's unknown dynamics or control laws that are difficult to be directly implemented, the nonlinear, strong coupling, and uncertainties of the model can be handled well to ensure the robust performance of the control law [6, 7]. For the rigid body model of AHV, the continuous and discrete adaptive neural controllers are designed, respectively, in [7, 8] by expressing original model as a strict feedback form and introducing RBFNN to approximate the model's unknown function, which guarantee that the closed-loop signals are uniformly ultimately bounded but fail to consider the influence of flexible states. Different from references [7, 8], a nonsingular direct neural control is proposed in [9] based on backstepping method by firstly designing the ideal backstepping control law for each subsystem of AHV and then using the RBFNN to approximate the designed ideal control law online instead of the unknown function of the model. However, the design process and form of the control law in [9] are cumbersome and complex, which restrict its applications in engineering. Two novel neural backstepping control strategies are proposed in [10, 11], which are designed with improved backstepping methods, respectively. Simulations show that the proposed methods in [10, 11] have strong robustness and superior control effects, but both of them assume that the model is affine for control input.

On the other hand, considering that AHV controls the height and attitude of longitudinal motion with elevators, as the flying height increases, the efficiency of the elevator will decrease significantly [12]. In addition, the AHV can be

affected by unknown airflows such as gust and turbulence during the flight process. Therefore, it is easy to encounter the phenomenon of elevator saturation when flying at high altitude. Once the actuators reach saturation, it may cause failure of the control system [13]. Thence, it requires urgent development of antisaturation control studies for AHV. However, the related research in this respect is still relatively little. Only considering the throttle setting constraint of the engine, a neural control method based on time-scale decomposition is designed in [14]. In [13], the neural network is used to approximate the saturation characteristics of the control law, which effectively solves the problem of control input constraint. However, the neural network weight parameters strongly depend on the model and are difficult to select. The tracking error is corrected through the designed auxiliary error compensation system in [15]. Although the simulation result shows that it has certain feasibility in dealing with the problem of actuator constraints, it cannot theoretically guarantee that the tracking error is bounded. The method of [15] is further extended to AHV flight control where both control input and flight attitudes are constrained. However, in the actual project, AHV has no corresponding actuators to directly limit its flight attitude.

There are two shortcomings in the above studies. First, forcing AHV's nonaffine motion model into an affine model will inevitably result in the loss of certain key dynamic characteristics. The control law designed based on the simplified affine model will have the risk of partial or complete failure. The second is that the difficulty of the controller design is increased to some extent by introducing the auxiliary system or using the neural network to approach the actuator saturation characteristic when dealing with the actuator constraints of the AHV.

Based on the above shortcomings, it is imperative to design a simple and effective nonaffine control law to solve the control problem of AHV when the actuators are constrained. This paper studies the control problem of AHV with actuator constraints and proposes an adaptive neural control method. By designing the hyperbolic tangent input saturation function, the original control problem with input constraints is transformed into a control problem without input constraints. Different from the above references, the AHV model is regarded as a pure feedback system with nonaffine control input that is closer to the actual situation of AHV. Based on the implicit function theorem, the RBFNN is introduced to accurately approximate the unknown function of the model. The MLP technique is adopted to adaptively adjust the norm of the weight vector, which greatly reduces the amount of adaptive calculations. And through employing FD to achieve effective estimation of the system state variables, the control accuracy is ensured. Simulation examples verify the effectiveness and superiority of the design method.

2. AHV Model and Preliminaries

2.1. Model Description. Parker, a scholar at the US Air Force Research Laboratory, based on the study of AHV models by Bolender and Doman [16] and by neglecting some slow dynamics and weak coupling of AHV, establishes the following AHV longitudinal motion model [17]:

$$\dot{V} = \frac{T\cos(\theta-\gamma) - D}{m} - g\sin\gamma, \tag{1}$$

$$\dot{h} = V\sin\gamma, \tag{2}$$

$$\dot{\gamma} = \frac{L + T\sin(\theta-\gamma)}{mV} - \frac{g}{V}\cos\gamma, \tag{3}$$

$$\dot{\theta} = Q, \tag{4}$$

$$\dot{Q} = \frac{M + \tilde{\psi}_1\ddot{\eta}_1 + \tilde{\psi}_2\ddot{\eta}_2}{I_{yy}}, \tag{5}$$

$$k_1\ddot{\eta}_1 = -2\zeta_1\omega_1\dot{\eta}_1 - \omega_1^2\eta_1 + N_1 - \tilde{\psi}_1\frac{M}{I_{yy}} - \frac{\tilde{\psi}_1\tilde{\psi}_2\ddot{\eta}_2}{I_{yy}}, \tag{6}$$

$$k_2\ddot{\eta}_2 = -2\zeta_2\omega_2\dot{\eta}_2 - \omega_2^2\eta_2 + N_2 - \tilde{\psi}_2\frac{M}{I_{yy}} - \frac{\tilde{\psi}_2\tilde{\psi}_1\ddot{\eta}_1}{I_{yy}}, \tag{7}$$

where

$$\begin{aligned} k_1 &= 1 + \frac{\tilde{\psi}_1}{I_{yy}}, \\ k_2 &= 1 + \frac{\tilde{\psi}_2}{I_{yy}}, \\ \tilde{\psi}_1 &= \int_{-L_f}^{0} \hat{m}_f\xi\phi_f(\xi)\mathrm{d}\xi, \\ \tilde{\psi}_2 &= \int_{0}^{L_a} \hat{m}_a\xi\phi_a(\xi)\mathrm{d}\xi, \end{aligned} \tag{8}$$

where velocity V, altitude h, flight-path γ, pitch angle θ, and pitch rate Q are the five rigid body states; m and I_{yy} represent vehicle mass and moment of inertia, respectively; the four flexible modes η_1, $\dot{\eta}_1$, η_2, and $\dot{\eta}_2$ denote the first two bending modes of the fuselage; ζ_i and $\omega_i (i = 1, 2)$ represent the damping ratio and natural frequency for flexible modes, respectively; L_f and L_a represent the length of forward beam and aft beam; $\hat{m}_f$ and $\hat{m}_a$ are the mass distribution of forward beam and aft beam, respectively; and $\phi_f(\cdot)$ and $\phi_a(\cdot)$ are structural mode shapes [16]. The force map of an AHV model is shown in Figure 1. The approximations of thrust T, drag D, lift L, pitching moment M, and the generalized forces $N_i (i = 1, 2)$ are expressed as [17]

$$T \approx C_T^{\alpha^3}\alpha^3 + C_T^{\alpha^2}\alpha^2 + C_T^{\alpha}\alpha + C_T^0,$$

$$D \approx \bar{q}S\left(C_D^{\alpha^2}\alpha^2 + C_D^{\alpha}\alpha + C_D^{\delta_e^2}\delta_e^2 + C_D^{\delta_e}\delta_e + C_D^0\right),$$

$$L \approx \bar{q}S\left(C_L^{\alpha}\alpha + C_L^{\delta_e}\delta_e + C_L^0\right),$$

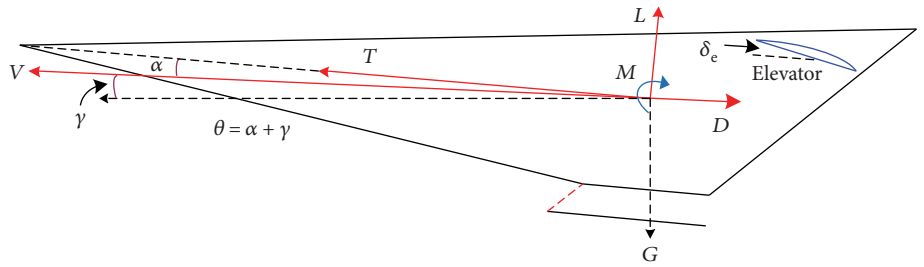

Figure 1: Force map of an AHV model.

$$
\begin{aligned}
M &\approx z_T T + \bar{q}S\bar{c}\left[C_{M,\alpha}^{\alpha^2}\alpha^2 + C_{M,\alpha}^{\alpha}\alpha + C_{M,\alpha}^{0} + c_e\delta_e\right],\\
N_1 &\approx N_1^{\alpha^2}\alpha^2 + N_1^{\alpha}\alpha + N_1^0,\\
N_2 &\approx N_2^{\alpha^2}\alpha^2 + N_2^{\alpha}\alpha + N_2^{\delta_e}\delta_e + N_2^0,\\
C_T^{\alpha^3} &= \beta_1(h,\bar{q})\Phi + \beta_2(h,\bar{q}),\\
C_T^{\alpha^2} &= \beta_3(h,\bar{q})\Phi + \beta_4(h,\bar{q}),\\
C_T^{\alpha} &= \beta_5(h,\bar{q})\Phi + \beta_6(h,\bar{q}),\\
C_T^{0} &= \beta_7(h,\bar{q})\Phi + \beta_8(h,\bar{q}),\\
\bar{q} &= \frac{1}{2}\overline{\rho}V^2,\\
\overline{\rho} &= \overline{\rho}_0 \exp\left(\frac{h_0 - h}{h_s}\right),
\end{aligned}
\tag{9}
$$

where $\alpha = \theta - \gamma$ is the angle of attack; fuel equivalence ratio Φ and elevator angular deflection δ_e are control inputs; $\bar{c}$ and S are the aerodynamic chord and reference area, respectively; $\bar{q}$ represents dynamic pressure; $\overline{\rho}$ is the air density at height h; z_T means thrust moment arm; c_e is the elevator coefficient; h_0 and $\overline{\rho}_0$ represent nominal altitude and air density at the altitude h_0, respectively; $1/h_s$ is the air density decay rate; $C_T^{\alpha^i}(i = 1, 2, 3)$ is the ith order coefficient of α in T; $C_D^{*^i}(i = 1, 2; * = \alpha, \delta_e)$ represents the ith order coefficient of $*$ in D; $C_L^{*}(* = \alpha, \delta_e)$ means coefficient of $*$ in L; $C_*^0(* = T, D, L)$ is the constant coefficient in $*$; $C_{M,\alpha}^{\alpha^i}(i = 0, 1, 2)$ represents the ith order coefficient of α in M; $N_j^{\alpha^i}(i = 0, 1, 2; j = 1, 2)$ is the ith order contribution of α to N_j; and $N_2^{\delta_e}$ is the contribution of δ_e to N_2; $\beta_i(h,\bar{q})(i = 1, 2, \ldots, 8)$ is the ith trust fit parameter. For more detailed definitions of the model geometric parameters and coefficients, the reader could refer to [17].

2.2. Input Constraint Problem and Model Conversion. According to [18] and combining (1), (2), (3), (4), (5), and (9), we know that velocity V is mainly controlled by equivalence ratio Φ since the thrust T is directly affected by Φ. On the other hand, altitude h is mainly controlled by elevator angular deflection δ_e since δ_e directly affects the pitch rate Q and then affects the pitch angle θ and flight-path γ, ultimately controlling the change of h. Therefore, we can firstly decompose the AHV model into a velocity subsystem (1) and altitude subsystem ((2), (3), (4), and (5)) and then design the control law separately [19].

Taking the actual situation into account, the executable ranges of Φ and δ_e have certain limits, which are described as follows:

$$
\begin{aligned}
\Phi &\in [\Phi_{\min}, \Phi_{\max}],\\
\delta_e &\in [\delta_{e\ \min}, \delta_{e\ \max}],
\end{aligned}
\tag{10}
$$

where $\Phi_{\min}$ and $\Phi_{\max} \geq 0$ are the respective upper and lower bound of Φ; $\delta_{e\ \min}$ and $\delta_{e\ \max}(\delta_{\text{emin}} = -\delta_{e\ \max})$ stand for the upper and lower bound of δ_e, respectively.

In the above situation of actuator constraints, for velocity subsystem and altitude subsystem, the control objective is to design the respective control law Φ and δ_e under the constraints of (10) such that V and h track their reference commands V_{ref} and h_{ref}.

Obviously, Φ and δ_e have saturation characteristics under the constraints of (10). In order to convert the original control problem with input constraints into a new control problem without input constraints, here we use hyperbolic tangent function to approximate Φ and δ_e

$$
\begin{aligned}
\Phi(\Phi^*) &= \frac{\Phi_{\max} - \Phi_{\min}}{2}\tanh\left(\frac{2\Phi^*}{\Phi_{\max} - \Phi_{\min}} - 1\right)\\
&\quad + \frac{\Phi_{\max} + \Phi_{\min}}{2},\\
\delta_e(\delta_e^*) &= \delta_{e\ \max}\tanh\left(\frac{\delta_e^*}{\delta_{e\ \max}}\right),
\end{aligned}
\tag{11}
$$

where Φ^* and $\delta_e^* \in \mathbf{R}$ are the actual input of actuator saturation loop. By (11) and the character of hyperbolic tangent function, we can know that no matter what values Φ^* and δ_e^* take, both Φ and δ_e satisfy the constraint of (10).

At this point, the original control objective can be converted to design unconstrained Φ^* and δ_e^* such that V and h track their reference commands V_{ref} and h_{ref}.

Remark 1. In order to maintain the normal operating mode of scramjet engine, a restriction is imposed on the value range

of Φ, which is generally taken as $\Phi \in [0.05, 1.5]$; taking the physical limit of the deflection angle of elevator into account, usually $\delta_e \in [-20^\circ, 20^\circ]$ [20].

Remark 2. Although the problem of actuator saturation is often considered when planning the trajectory, AHV can be affected by unknown airflows such as gusts and turbulences as well as sudden actuator failures during the flight process, which will cause the actuator to be saturated instantly such that the actual executable range of it will be even smaller than its theoretical value [13].

3. Adaptive Neural Controller Design

3.1. RBFNN Approximation. RBFNN has the characteristics of simple structure, strong learning, and fault tolerance and has the ability of globally approximating nonlinear continuous functions [21]. It can be expressed as a mapping from input to output.

$$y = \mathbf{W}^{\mathrm{T}}\mathbf{h}(\mathbf{X}), \tag{12}$$

where $\mathbf{X} = [X_1, X_2, \ldots, X_n]^{\mathrm{T}} \in \mathbf{R}^n$ is the input vector (n represents the dimension of the input vector), $\mathbf{W} = [w_1, w_2, \ldots, w_N]^{\mathrm{T}} \in \mathbf{R}^N$ stands for the weight vector (N is the number of hidden layer nodes), $\mathbf{h}(\mathbf{X}) = [h_1(\mathbf{X}), h_2(\mathbf{X}), \ldots, h_N(\mathbf{X})]^{\mathrm{T}} \in \mathbf{R}^N$, $h_i(\mathbf{X})$, denotes the activation function. Here, $h_i(\mathbf{X})$ is chosen as the following Gaussian function:

$$h_i(\mathbf{X}) = \exp\left(-\frac{\|\mathbf{X} - \mathbf{c}_i\|^2}{2b_i^2}\right), \quad i = 1, 2, \ldots, N, \tag{13}$$

where $\mathbf{b} = [b_1, b_2, \ldots, b_N]^{\mathrm{T}} \in \mathbf{R}^N$, b_i, is the width of the ith Gaussian function; $\mathbf{c} = [\mathbf{c}_1, \mathbf{c}_2, \ldots, \mathbf{c}_N] \in \mathbf{R}^{n\times N}$ ($\mathbf{c}_i$ represents the center of the ith Gaussian function), which can be expressed as follows:

$$\mathbf{c} = \begin{bmatrix} c_{11} & \cdots & c_{1N} \\ \vdots & \ddots & \vdots \\ c_{n1} & \cdots & c_{nN} \end{bmatrix}. \tag{14}$$

For any unknown nonlinear continuous function $F(\mathbf{X})$, using the RBFNN and by selecting enough nodes (selecting a sufficiently large N), there must be an ideal weight vector $\mathbf{W}^* = [w_1^*, w_2^*, \ldots, w_N^*]^{\mathrm{T}} \in \mathbf{R}^N$ that satisfies [21]

$$F(\mathbf{X}) = \mathbf{W}^{*\mathrm{T}}\mathbf{h}(\mathbf{X}) + \mu, \quad |\mu| \le \mu_{\mathrm{M}}, \tag{15}$$

where $\mu \in \mathbf{R}$ is the approximation error and $\mu_{\mathrm{M}} \in \mathbf{R}^+$ stands for the upper bound of approximation error. When taking N large enough, μ_{M} can be arbitrarily small.

Remark 3. Since $\exp(\cdot)$ is a strictly monotonically increasing and positive function and $-\|\mathbf{X} - \mathbf{c}_i\|^2/(2b_i^2) \le 0$, there is $0 < h_i(\mathbf{X}) \le h_i(0) = 1$. Therefore, there must be a bounded constant $\bar{h} \in \mathbf{R}^+$ such that $\|\mathbf{h}(\mathbf{X})\| \le \bar{h}$.

3.2. Controller Design for Velocity Subsystem. Based on the research conclusion of [7], here velocity subsystem is further expressed as a more general nonaffine form of control input

$$\dot{V} = F_V(V, \Phi). \tag{16}$$

Combined with (11), the above formula can be rewritten as

$$\dot{V} = F_V(V, \Phi^*), \tag{17}$$

where $F_V(V, \Phi^*)$ is a completely unknown continuously differentiable function.

In order to design the control law Φ^*, the following theorem is given firstly.

Theorem 1. *For any $(V, \Phi^*) \in \Omega_V \times \mathbf{R}$, the following inequality is established:*

$$\frac{\partial F_V(V, \Phi^*)}{\partial \Phi^*} > 0, \tag{18}$$

where Ω_V is a controllable area.

Proof 1. From (11), (16), and (17), we can know

$$\begin{aligned} \frac{\partial F_V(V, \Phi^*)}{\partial \Phi^*} &= \frac{\partial F_V(V, \Phi^*)}{\partial \Phi} \cdot \frac{\partial \Phi}{\partial \Phi^*} \\ &= \frac{((\partial F_V(V, \Phi))/\partial \Phi)}{\cosh^2((2\Phi^*/(\Phi_{\max} - \Phi_{\min})) - 1)}. \end{aligned} \tag{19}$$

According to [17], there is

$$\frac{\partial F_V(V, \Phi)}{\partial \Phi} > 0. \tag{20}$$

Therefore,

$$\frac{\partial F_V(V, \Phi^*)}{\partial \Phi^*} > 0. \tag{21}$$

Define velocity tracking error

$$\tilde{V} = V - V_{\mathrm{ref}}. \tag{22}$$

Taking time derivative along (22) and using (17) yield

$$\dot{\tilde{V}} = \dot{V} - \dot{V}_{\mathrm{ref}} = F_V(V, \Phi^*) - \dot{V}_{\mathrm{ref}}. \tag{23}$$

Let

$$F_V^*(V, \Phi^*) = F_V(V, \Phi^*) - k_V\Phi^*. \tag{24}$$

where $k_V \in \mathbf{R}^+$ is the design parameter.

Combine (23) and (24)

$$\dot{\tilde{V}} = \dot{V} - \dot{V}_{\text{ref}} = F_V^*(V, \Phi^*) + k_V \Phi^* - \dot{V}_{\text{ref}}. \tag{25}$$

Design the control law Φ^* as

$$\Phi^* = {k_V}^{-1}(\Phi_0^* - \Phi_1^*), \tag{26}$$

where

$$\Phi_0^* = -k_{V1}\tilde{V} - k_{V2}\int_0^t \tilde{V} d\tau + \dot{V}_{\text{ref}}. \tag{27}$$

k_{V1} and $k_{V2} \in \mathbf{R}^+$ stand for design parameters and Φ_1^* is the neural control law to be designed to counteract the influence of uncertain term $F_V^*(V, \Phi^*)$.

In order to facilitate the subsequent design process, the implicit function theorem is introduced here [22].

Theorem 2. *Assume that the implicit function $\Psi : \mathbf{R}^l \times \mathbf{R}^r \to \mathbf{R}^l$ is continuously differentiable at each point (ς, σ) on the open set $Y \subset \mathbf{R}^l \times \mathbf{R}^r$. (ς_0, σ_0) is the point in Y; $\Psi(\varsigma_0, \sigma_0) = 0$ and the Jacobian matrix $(\partial\Psi/\partial\varsigma)(\varsigma_0, \sigma_0)$ is nonsingular. Then, for any $\sigma \in G$, a neighborhood $U \subset \mathbf{R}^l$ of ς_0 and a neighborhood $G \subset \mathbf{R}^r$ of σ_0 can make the equation $\Psi(\varsigma, \sigma) = 0$ which has a unique solution $\varsigma \in U$, and the solution can be expressed as $\varsigma = g_0(\sigma)$, where $g_0(\cdot)$ is a continuously differentiable function on $\sigma = \sigma_0$.*

Remark 4. Theorem 2 shows that once the implicit function $\Psi(\varsigma, \sigma)$ satisfies all conditions in the theorem, ς can be expressed as a continuously differentiable function of σ, that is, $\varsigma = g_0(\sigma)$. At this time, using RBFNN to approximate $\Psi(\varsigma, \sigma)$, only σ, instead of ς, is used as the input signal of the neural network to obtain a satisfactory approximation effect. This is where the special meaning of the implicit function theorem lies.

Let

$$\begin{aligned}\Gamma(V, \Phi_0^*, \Phi_1^*) &\triangleq F_V^*(V, \Phi^*) - \Phi_1^* \\ &= F_V^*\left(V, {k_V}^{-1}(\Phi_0^* - \Phi_1^*)\right) - \Phi_1^*.\end{aligned} \tag{28}$$

To illustrate that $\Gamma(V, \Phi_0^*, \Phi_1^*)$ satisfies the implicit function theorem, the following theorem is given.

Theorem 3. *Define*

$$k_V > \frac{1}{2}\frac{\partial F_V(V, \Phi^*)}{\partial \Phi^*}. \tag{29}$$

Then there are a controllable area $\Omega_V \subset \mathbf{R}$ and a unique Φ_1^* for any $(V, \Phi_1^*) \in \Omega_V \times \mathbf{R}$; Φ_1^* satisfies

$$\Gamma(V, \Phi_0^*, \Phi_1^*) = 0. \tag{30}$$

Proof 2. According to [23], a sufficient condition for the existence of Φ_1^* is that the following inequality holds:

$$\left|\frac{\partial F_V^*(V, \Phi^*)}{\partial \Phi_1^*}\right| < 1. \tag{31}$$

Consider (18), (24), (26), and (29), there are

$$\begin{aligned}\left|\frac{\partial F_V^*(V, \Phi^*)}{\partial \Phi_1^*}\right| &= \left|\frac{\partial[F_V(V, \Phi^*) - k_V\Phi^*]}{\partial \Phi_1^*}\right| \\ &= \left|\frac{\partial[F_V(V, \Phi^*) - k_V\Phi^*]}{\partial \Phi^*}\frac{\partial \Phi^*}{\partial \Phi_1^*}\right| \\ &= \left|\left[\frac{\partial F_V(V, \Phi^*)}{\partial \Phi^*} - k_V\right]\frac{1}{k_V}\right| \\ &= \left|\frac{1}{k_V}\frac{\partial F_V(V, \Phi^*)}{\partial \Phi^*} - 1\right| < 1.\end{aligned} \tag{32}$$

Therefore, Φ_1^* exists.

Further,

$$\begin{aligned}\frac{\partial \Gamma(V, \Phi_0^*, \Phi_1^*)}{\partial \Phi_1^*} &= \frac{\partial[F_V^*(V, \Phi^*) - \Phi_1^*]}{\partial \Phi_1^*} \\ &= \frac{\partial[F_V(V, \Phi^*) - k_V\Phi^*]}{\partial \Phi_1^*} - 1 \\ &= \frac{\partial[F_V(V, \Phi^*) - k_V\Phi^*]}{\partial \Phi^*}\frac{\partial \Phi^*}{\partial \Phi_1^*} - 1 \\ &= \left[\frac{\partial F_V(V, \Phi^*)}{\partial \Phi^*} - k_V\right]\left(-\frac{1}{k_V}\right) - 1 \\ &= -\frac{1}{k_V}\frac{\partial F_V(V, \Phi^*)}{\partial \Phi^*},\end{aligned} \tag{33}$$

where $\Phi^* = {k_V}^{-1}(\Phi_0^* - \Phi_1^*)$.

Combine (18) and (33)

$$\frac{\partial \Gamma(V, \Phi_0^*, \Phi_1^*)}{\partial \Phi_1^*} < 0. \tag{34}$$

According to Theorem 3 and (34), $\Gamma(V, \Phi_0^*, \Phi_1^*)$ satisfies the implicit function theorem. Therefore, Φ_1^* can be regarded as a function of Φ_0^* and V, and further $F_V^*(V, \Phi^*)$ can be regarded as a function of Φ_0^* and V.

Define $\mathbf{X}_1 = [V, \Phi_0^*]^{\mathrm{T}} \in \mathbf{R}^2$ as the input vector of RBFNN and introduce RBFNN to approximate $F_V^*(V, \Phi^*)$

$$F_V^*(V, \Phi^*) = \mathbf{W}_V^{*\mathrm{T}}\mathbf{h}(\boldsymbol{X}_1) + \varepsilon, \quad |\varepsilon| \le \varepsilon_M, \tag{35}$$

where $\mathrm{W}_V^{*\mathrm{T}} = [w_{V1}^*, w_{V2}^*, \ldots, w_{VN_1}^*]^{\mathrm{T}} \in \mathbf{R}^{N_1}$ is the weight vector, N_1 is the number of nodes, and ε and ε_M are approximation errors and its upper bounds, respectively. And $\mathbf{h}(\boldsymbol{X}_1) = [h_1(\mathbf{X}_1), h_2(\mathbf{X}_1), \ldots, h_{N_1}(\mathbf{X}_1)]^{\mathrm{T}} \in \mathbf{R}^{N_1}$, where $h_i(\mathbf{X}_1)$ is the activation function; here, $h_i(\mathbf{X}_1)$ is chosen as the Gaussian function.

The following is based on the MLP technique to adaptively adjust the norm of the RBFNN weight vector.

Define $\omega_V = \|\mathbf{W}_V^*\|^2$ and design Φ_1^* as

$$\Phi_1^* = \frac{1}{2}\tilde{V}\widehat{\omega}_V \mathbf{h}^{\mathrm{T}}(\mathbf{X}_1)\mathbf{h}(\mathrm{X}_1), \tag{36}$$

where $\widehat{\omega}_V$ is the estimation of ω_V, and its adaptive law is designed as

$$\dot{\widehat{\omega}}_V = \frac{\mu_V}{2}\tilde{V}^2\mathbf{h}^{\mathrm{T}}(\mathbf{X}_1)\mathbf{h}(\mathbf{X}_1) - 2\widehat{\omega}_V, \tag{37}$$

where $\mu_V \in \mathbf{R}^+$ is the design parameter.

Substitute (27) and (36) into (26) and finally get the control law Φ^*

$$\Phi^* = k_V^{-1}\left[-k_{V1}\tilde{V} - k_{V2}\int_0^t \tilde{V}d\tau + \dot{V}_{\mathrm{ref}} - \frac{1}{2}\tilde{V}\widehat{\omega}_V\mathbf{h}^{\mathrm{T}}(\mathbf{X}_1)\mathbf{h}(\mathbf{X}_1)\right]. \tag{38}$$

Remark 5. Different from [24] in which the weight vector of the neural network is directly adjusted online, this paper regards $\mathbf{W}_V^*$ as a whole based on the MLP technique. Adaptive adjustment of ω_V requires only one online learning parameter $\widehat{\omega}_V$, and the computational complexity of the approximation algorithm is significantly reduced.

3.3. Controller Design for Altitude Subsystem. Define altitude tracking error

$$\tilde{h} = h - h_{\mathrm{ref}}. \tag{39}$$

Taking time derivative along (39) and using (2) yield

$$\dot{\tilde{h}} = V\sin\gamma - \dot{h}_{\mathrm{ref}}. \tag{40}$$

The reference trajectory of γ is chosen as

$$\gamma_{\mathrm{d}} = \arcsin\left(\frac{-k_{\gamma 1}\tilde{h} - k_{\gamma 2}\int_0^t \tilde{h}\mathrm{d}\tau + \dot{h}_{\mathrm{ref}}}{V}\right), \tag{41}$$

where $k_{\gamma 1}$, and $k_{\gamma 2} \in \mathbf{R}^+$ are design parameters. If $\gamma \to \gamma_{\mathrm{d}}$, known by (40) and (41), the dynamic response of $\tilde{h}$ is

$$\ddot{\tilde{h}} + k_{\gamma 1}\dot{\tilde{h}} + k_{\gamma 2}\tilde{h} = 0. \tag{42}$$

Performing Laplace transformation on both sides of (42) can get its characteristic equation

$$s^2 + k_{\gamma 1}s + k_{\gamma 2} = 0. \tag{43}$$

The two characteristic roots $(-k_{\gamma 1} - \sqrt{{k_{\gamma 1}}^2 - 4k_{\gamma 2}})/2$ and $(-k_{\gamma 1} + \sqrt{{k_{\gamma 1}}^2 - 4k_{\gamma 2}})/2$ of (43) are negative real numbers, so the system (42) is stable and $\tilde{h}$ is exponentially convergent. Therefore, as long as $\gamma \to \gamma_{\mathrm{d}}$, h can track h_{ref} stably. In this way, the control objective of the altitude subsystem turns to ensure that γ tracks γ_{d}.

Define $x_1 = \gamma$, $x_2 = \theta$, and $x_3 = Q$. Based on the research conclusion of [7], the remaining part of the altitude subsystem ((3), (4), and (5)) is further expressed as the following more general nonaffine form:

$$\begin{aligned}\dot{x}_1 &= f_1(x_1, x_2),\\ \dot{x}_2 &= x_3,\\ \dot{x}_3 &= f_3(\mathbf{x}, \delta_{\mathrm{e}}).\end{aligned} \tag{44}$$

Considering (11), the above formula can be rewritten as

$$\begin{aligned}\dot{x}_1 &= f_1(x_1, x_2),\\ \dot{x}_2 &= x_3,\\ \dot{x}_3 &= f_3(\mathbf{x}, \delta_{\mathrm{e}}^*),\end{aligned} \tag{45}$$

where $\mathbf{x} = [x_1, x_2, x_3]^{\mathrm{T}}$. $f_1(x_1, x_2)$ and $f_3(\mathbf{x}, \delta_{\mathrm{e}}^*)$ are completely unknown continuously differentiable functions.

Remark 6. Due to the strong coupling between the rigid body states and the flexible modes in the AHV model ((1), (2), (3), (4), (5), (6), and (7)), here the dynamic characteristics of strong nonlinearity and strong coupling in the original model are regarded as completely unknown continuous differentiable functions ((16) and (44)) by referring to the method of [25]. The proposed method in this paper will use RBFNN to accurately approximate these continuous differentiable functions and then complete the design of the control law and ensure the stability of the closed-loop control system.

In order to design the control law δ_{e}^*, the following theorem is given firstly.

Theorem 4. *For any* $(\boldsymbol{x}, \delta_{\mathrm{e}}^*) \in \Omega_{\boldsymbol{x}} \times \mathbf{R}$*, the following inequalities are established:*

$$\begin{aligned}\frac{\partial f_1(x_1, x_2)}{\partial x_2} &> 0,\\ \frac{\partial f_3(\mathbf{x}, \delta_{\mathrm{e}}^*)}{\partial \delta_{\mathrm{e}}^*} &> 0,\end{aligned} \tag{46}$$

where $\Omega_{\boldsymbol{x}}$ *is a controllable area.*

Proof 3. According to the results in [17], we can know

$$\begin{aligned}\frac{\partial f_1(x_1, x_2)}{\partial x_2} &> 0,\\ \frac{\partial f_3(\mathbf{x}, \delta_{\mathrm{e}})}{\partial \delta_{\mathrm{e}}} &> 0.\end{aligned} \tag{47}$$

Consider (11), (44) and (45), there is

$$\frac{\partial f_3(\mathbf{x},\delta_e^*)}{\partial \delta_e^*} = \frac{\partial f_3(\mathbf{x},\delta_e^*)}{\partial \delta_e} \cdot \frac{\partial \delta_e}{\partial \delta_e^*} = \frac{(\partial f_3(\mathbf{x},\delta_e))/\partial \delta_e}{\cosh^2(\delta_e^*/\delta_{emax})}. \tag{48}$$

Combining (47) and (48), we can see that (46) is true.

In order to avoid the cumbersome and complicated design process of the traditional backstepping method in designing the control law, the following equivalent transformation is performed on the system (45).

Step 1. Let $z_1 = x_1 = \gamma$ and $z_2 = \dot{z}_1 = f_1(x_1, x_2)$. From (45), the time derivative of z_2 is derived as

$$\begin{aligned}\dot{z}_2 &= \frac{\partial f_1(x_1,x_2)}{\partial x_1}\dot{x}_1 + \frac{\partial f_1(x_1,x_2)}{\partial x_2}\dot{x}_2 \\ &= \frac{\partial f_1(x_1,x_2)}{\partial x_1} f_1(x_1,x_2) + \frac{\partial f_1(x_1,x_2)}{\partial x_2} x_3 \\ &\triangleq f_{h1}(\mathbf{x}).\end{aligned} \tag{49}$$

Step 2. Let $z_3 = \dot{z}_2 = f_{h1}(\mathbf{x})$. From (45), the time derivative of z_3 is derived as

$$\begin{aligned}\dot{z}_3 &= \frac{\partial f_{h1}(\mathbf{x})}{\partial x_1}\dot{x}_1 + \frac{\partial f_{h1}(\mathbf{x})}{\partial x_2}\dot{x}_2 + \frac{\partial f_{h1}(\mathbf{x})}{\partial x_3}\dot{x}_3 \\ &= \frac{\partial f_{h1}(\mathbf{x})}{\partial x_1} f_1(x_1,x_2) + \frac{\partial f_{h1}(\mathbf{x})}{\partial x_2} x_3 + \frac{\partial f_{h1}(\mathbf{x})}{\partial x_3} f_3(\mathbf{x},\delta_e^*) \\ &\triangleq f_{h2}(\mathbf{x},\delta_e^*).\end{aligned} \tag{50}$$

After the above transformation, system (45) is as follows:

$$\begin{aligned}\dot{z}_1 &= z_2, \\ \dot{z}_2 &= z_3, \\ \dot{z}_3 &= f_{h2}(\mathbf{x},\delta_e^*),\end{aligned} \tag{51}$$

where $f_{h2}(\mathbf{x},\delta_e^*)$ is a completely unknown continuously differentiable function.

Remark 7. From (46), (49) and (50), there is

$$\begin{aligned}\frac{\partial f_{h2}(\mathbf{x},\delta_e^*)}{\partial \delta_e^*} &= \frac{\partial f_{h1}(\mathbf{x})}{\partial x_3}\frac{\partial f_3(\mathbf{x},\delta_e^*)}{\partial \delta_e^*} \\ &= \frac{\partial f_1(x_1,x_2)}{\partial x_2}\frac{\partial f_3(\mathbf{x},\delta_e^*)}{\partial \delta_e^*} > 0.\end{aligned} \tag{52}$$

Define flight-path tracking error e and error function E

$$\begin{aligned}e &= \gamma - \gamma_d = z_1 - \gamma_d, \\ E &= \left(\frac{d}{dt} + \lambda\right)^3 \int_0^t e d\tau = \ddot{e} + 3\lambda\dot{e} + 3\lambda^2 e + \lambda^3 \int_0^t e d\tau,\end{aligned} \tag{53}$$

where $\lambda \in \mathbf{R}^+$ stands for the design parameter. Since $(s+\lambda)^3$ is a Hurwitz polynomial, when E is bounded, e must be bounded.

According to (51) and (53), we obtain

$$\begin{aligned}\dot{e} &= \dot{z}_1 - \dot{\gamma}_d = z_2 - \dot{\gamma}_d, \\ \ddot{e} &= \dot{z}_2 - \ddot{\gamma}_d = z_3 - \ddot{\gamma}_d, \\ \dddot{e} &= \dot{z}_3 - \dddot{\gamma}_d = f_{h2}(\mathbf{x},\delta_e^*) - \dddot{\gamma}_d.\end{aligned} \tag{54}$$

Considering that z_2 and z_3 are unknown, we can know that $z_2 = \dot{\gamma}$ and $z_3 = \ddot{\gamma}$ from the previous model transformation process. A new finite-time convergence differentiator (FD) will be used below to accurately estimate differential signal. By taking γ as the input signal of FD (take $n = 4$), we can get the estimated values of z_2 and z_3, which are expressed as $\hat{z}_2$ and $\hat{z}_3$, respectively. Similarly, the estimations of $\dot{\gamma}_d$, $\ddot{\gamma}_d$, and $\dddot{\gamma}_d$ can be obtained via taking γ_d as the input signal of FD (take $n = 4$), which are expressed as $\hat{\dot{\gamma}}_d$, $\hat{\ddot{\gamma}}_d$, and $\hat{\dddot{\gamma}}_d$.

Therefore, the estimations of the first three derivatives of e can be expressed as

$$\begin{aligned}\hat{\dot{e}} &= \hat{z}_2 - \hat{\dot{\gamma}}_d, \\ \hat{\ddot{e}} &= \hat{z}_3 - \hat{\ddot{\gamma}}_d, \\ \hat{\dddot{e}} &= f_{h2}(\mathbf{x},\delta_e^*) - \hat{\dddot{\gamma}}_d.\end{aligned} \tag{55}$$

From (53) and (55), we obtain the estimation of E

$$\hat{E} = \hat{\ddot{e}} + 3\lambda\hat{\dot{e}} + 3\lambda^2 e + \lambda^3 \int_0^t e d\tau. \tag{56}$$

Let

$$F_h(\mathbf{x},\delta_e^*) = f_{h2}(\mathbf{x},\delta_e^*) - k_h\delta_e^*, \tag{57}$$

where $k_h \in \mathbf{R}^+$ is the design parameter.

Combine (55), (56), and (57)

$$\dot{\hat{E}} = k_h\delta_e^* + F_h(\mathbf{x},\delta_e^*) - \hat{\dddot{\gamma}}_d + 3\lambda\hat{\ddot{e}} + 3\lambda^2\hat{\dot{e}} + \lambda^3 e. \tag{58}$$

Design the control law δ_e^* as

$$\delta_e^* = k_h^{-1}(\delta_{e0}^* - \delta_{e1}^*), \tag{59}$$

where $\delta_{e0}^* = -k_{h1}\hat{E} + \hat{\dddot{\gamma}}_d - 3\lambda\hat{\ddot{e}} - 3\lambda^2\hat{\dot{e}} - \lambda^3 e$, $k_{h1} \in \mathbf{R}^+$ represents the design parameter, and δ_{e1}^* is the neural control law to be designed to counteract the influence of the uncertain term $F_h(\mathbf{x},\delta_e^*)$.

Let

$$\begin{aligned}H(\mathbf{x},\delta_{e0}^*,\delta_{e1}^*) &\triangleq F_h(\mathbf{x},\delta_e^*) - \delta_{e1}^* \\ &= F_h\left(\mathbf{x}, k_h^{-1}(\delta_{e0}^* - \delta_{e1}^*)\right) - \delta_{e1}^*.\end{aligned} \tag{60}$$

Similar to velocity subsystem, to illustrate that $H(\mathbf{x}, \delta_{e0}^*, \delta_{e1}^*)$ satisfies the implicit function theorem, the following theorem is given.

Theorem 5. *If*

$$k_h > \frac{1}{2}\frac{\partial f_{h2}(\mathbf{x}, \delta_e^*)}{\partial \delta_e^*}, \tag{61}$$

then there are a controllable area $\Omega_h \subset \mathbf{R}^3$ *and a unique* δ_{e1}^* *for any* $(\mathbf{x}, \delta_{e1}^*) \in \Omega_h \times \mathbf{R}$; δ_{e1}^* *satisfies*

$$H(\mathbf{x}, \delta_{e0}^*, \delta_{e1}^*) = 0. \tag{62}$$

Proof 4. From [23], a sufficient condition for the existence of δ_{e1}^* is that the following inequality holds:

$$\left|\frac{\partial F_h(\mathbf{x}, \delta_e^*)}{\partial \delta_{e1}^*}\right| < 1. \tag{63}$$

Consider (52), (59) and (61), there are

$$\begin{aligned}\left|\frac{\partial F_h(\mathbf{x}, \delta_e^*)}{\partial \delta_{e1}^*}\right| &= \left|\frac{\partial [f_{h2}(\mathbf{x}, \delta_e^*) - k_h \delta_e^*]}{\partial \delta_{e1}^*}\right| \\ &= \left|\frac{\partial [f_{h2}(\mathbf{x}, \delta_e^*) - k_h \delta_e^*]}{\partial \delta_e^*}\frac{\partial \delta_e^*}{\partial \delta_{e1}^*}\right| \\ &= \left|\left[\frac{\partial f_{h2}(\mathbf{x}, \delta_e^*)}{\partial \delta_e^*} - k_h\right]\frac{1}{k_h}\right| \\ &= \left|\frac{1}{k_h}\frac{\partial f_{h2}(\mathbf{x}, \delta_e^*)}{\partial \delta_e^*} - 1\right| < 1.\end{aligned} \tag{64}$$

Therefore, δ_{e1}^* exists.

Further,

$$\begin{aligned}\frac{\partial}{\partial \delta_{e1}^*} H(\mathbf{x}, \delta_{e0}^*, \delta_{e1}^*) &= \frac{\partial}{\partial \delta_{e1}^*}[F_h(\mathbf{x}, \delta_e^*) - \delta_{e1}^*] \\ &= \frac{\partial}{\partial \delta_{e1}^*}[f_{h2}(\mathbf{x}, \delta_e^*) - k_h \delta_e^*] - 1 \\ &= \frac{\partial}{\partial \delta_e^*}[f_{h2}(\mathbf{x}, \delta_e^*) - k_h \delta_e^*]\frac{\partial \delta_e^*}{\partial \delta_{e1}^*} - 1 \\ &= \left[\frac{\partial f_{h2}(\mathbf{x}, \delta_e^*)}{\partial \delta_e^*} - k_h\right]\left(-\frac{1}{k_h}\right) - 1 \\ &= -\frac{1}{k_h}\frac{\partial f_{h2}(\mathbf{x}, \delta_e^*)}{\partial \delta_e^*}.\end{aligned} \tag{65}$$

Combine (52) and (65)

$$\frac{\partial}{\partial \delta_{e1}^*} H(\mathbf{x}, \delta_{e0}^*, \delta_{e1}^*) < 0 \tag{66}$$

According to Theorem 5 and (66), $H(\mathbf{x}, \delta_{e0}^*, \delta_{e1}^*)$ satisfies the implicit function theorem. Therefore, δ_{e1}^* can be regarded as a function of δ_{e0}^* and $\mathbf{x}$, and further $F_h(\mathbf{x}, \delta_e^*)$ can be regarded as a function of δ_{e0}^* and $\mathbf{x}$.

Define $\mathbf{X}_2 = [\mathbf{x}^{\mathrm{T}}, \delta_{e0}^*]^{\mathrm{T}} \in \mathbf{R}^4$ as the input vector of RBFNN and introduce RBFNN to approximate $F_h(\mathbf{x}, \delta_e^*)$

$$F_h(\mathbf{x}, \delta_e^*) = \mathbf{W}_h^{*\mathrm{T}}\mathbf{h}(\mathbf{X}_2) + \iota, \quad |\iota| \le \iota_{\mathrm{M}}, \tag{67}$$

where $\mathbf{W}_h^{*\mathrm{T}} = [w_{h1}^*, w_{h2}^*, \dots, w_{hN_2}^*]^{\mathrm{T}} \in \mathbf{R}^{N_2}$ is the weight vector, N_2 is the number of nodes, and ι and ι_{M} stand for approximation errors and its upper bounds, respectively. $\mathbf{h}(\mathbf{X}_2) = [h_1(\mathbf{X}_2), h_2(\mathbf{X}_2), \dots, h_{N_1}(\mathbf{X}_2)]^{\mathrm{T}} \in \mathbf{R}^{N_2}$, $h_i(\mathbf{X}_2)$, is the activation function which is chosen as the Gaussian function here.

Define $\omega_h = \|\mathbf{W}_h^*\|^2$ and design δ_{e1}^* as

$$\delta_{e1}^* = \frac{1}{2}\widehat{E}\widehat{\omega}_h \mathbf{h}^{\mathrm{T}}(\mathbf{X}_2)\mathbf{h}(\mathbf{X}_2), \tag{68}$$

where $\widehat{\omega}_h$ is the estimation of ω_h, and its adaptive law is designed as

$$\dot{\widehat{\omega}}_h = \frac{\mu_h}{2}\widehat{E}^2 \mathbf{h}^{\mathrm{T}}(\boldsymbol{X}_2)\mathbf{h}(\mathbf{X}_2) - 2\widehat{\omega}_h, \tag{69}$$

where $\mu_h \in \mathbf{R}^+$ is the design parameter.

3.4. Finite-Time Convergence Differentiator (FD)

Theorem 6. *Consider the following FD [26]:*

$$\begin{aligned}\dot{\xi}_1 &= \xi_2, \\ \dot{\xi}_2 &= \xi_3, \\ &\vdots \\ \dot{\xi}_{n-1} &= \xi_n, \\ \dot{\xi}_n &= R^n\left[-a_1 \arctan(\xi_1 - \upsilon(t)) - a_2 \arctan\left(\frac{\xi_2}{R}\right)\right. \\ &\qquad \left. - \cdots - a_n \arctan\left(\frac{\xi_n}{R^{n-1}}\right)\right],\end{aligned} \tag{70}$$

where $R, a_i\ (i = 1, 2, \dots, n) \in \mathbf{R}^+$ *stand for the design parameters. There are* $\phi > 0$ *and* $\iota\phi > n$ *so that*

$$\xi_i - \upsilon^{(i-1)}(t) = O\left(\left(\frac{1}{R}\right)^{\iota\phi - i + 1}\right), \quad i = 1, 2, \dots, n, \tag{71}$$

where $O((1/R)^{\iota\phi - i + 1})$ *denotes the approximation of* $(1/R)^{\tau\phi - i + 1}$ *order between* ξ_i *and* $\upsilon^{(i-1)}(t)$, $\phi = (1 - \vartheta)/\vartheta$, $\vartheta \in (0, \min\{\iota/(\iota + n), 1/2\})$, $n \ge 2$.

Proof 5. The detailed proof process of Theorem 6 can be found in [26].

Remark 8. In (70), $\xi_i\,(i=1,2,\dots,n)$ is the state variable of the system, ξ_1 is the estimation of $v(t)$, and $\xi_i\,(i=2,3,\dots,n)$ is the estimation of the $i-1$th derivative of $v(t)$. At the same time, (71) shows that the estimation error is a high-order infinitesimal of $(1/R)^{\tau\phi-i+1}$.

Use the above FD to estimate z_2, z_3, $\dot{\gamma}_{\mathrm{d}}$, $\ddot{\gamma}_{\mathrm{d}}$, and $\dddot{\gamma}_{\mathrm{d}}$ of (54)

$$\begin{aligned}
\dot{\widehat{z}}_1 &= \widehat{z}_2,\\
\dot{\widehat{z}}_2 &= \widehat{z}_3,\\
\dot{\widehat{z}}_3 &= \widehat{z}_4,\\
\dot{\widehat{z}}_4 &= R_1^4\left[-a_{11}\arctan\left(\widehat{z}_1-\gamma\right)-a_{12}\arctan\left(\frac{\widehat{z}_2}{R_1}\right)\right.\\
&\qquad \left.-a_{13}\arctan\left(\frac{\widehat{z}_3}{R_1^2}\right)-a_{14}\arctan\left(\frac{\widehat{z}_4}{R_1^3}\right)\right],\\
\left(\widehat{\gamma}_{\mathrm{d}}\right)' &= \dot{\widehat{\gamma}}_{\mathrm{d}},\\
\left(\dot{\widehat{\gamma}}_{\mathrm{d}}\right)' &= \ddot{\widehat{\gamma}}_{\mathrm{d}},\\
\left(\ddot{\widehat{\gamma}}_{\mathrm{d}}\right)' &= \dddot{\widehat{\gamma}}_{\mathrm{d}},\\
\left(\dddot{\widehat{\gamma}}_{\mathrm{d}}\right)' &= R_2^4\left[-a_{21}\arctan\left(\widehat{\gamma}_{\mathrm{d}}-\gamma_{\mathrm{d}}\right)-a_{22}\arctan\left(\frac{\dot{\widehat{\gamma}}_{\mathrm{d}}}{R_2}\right)\right.\\
&\qquad \left.-a_{23}\arctan\left(\frac{\ddot{\widehat{\gamma}}_{\mathrm{d}}}{R_1^2}\right)-a_{24}\arctan\left(\frac{\dddot{\widehat{\gamma}}_{\mathrm{d}}}{R_2^3}\right)\right],
\end{aligned} \tag{72}$$

where $R_i, a_{ij}\,(i=1,2;j=1,2,3,4)\in\mathbf{R}^+$ are design parameters; $\widehat{z}_1$, $\widehat{z}_2$, $\widehat{z}_3$, and $\widehat{z}_4$ represent the estimations of $z_1(\gamma)$, $z_2(\dot{\gamma})$, $z_3(\ddot{\gamma})$, and $z_4(\dddot{\gamma})$, respectively; and $\widehat{\gamma}_{\mathrm{d}}$, $\dot{\widehat{\gamma}}_{\mathrm{d}}$, $\ddot{\widehat{\gamma}}_{\mathrm{d}}$, and $\dddot{\widehat{\gamma}}_{\mathrm{d}}$ stand for the estimations of γ_{d}, $\dot{\gamma}_{\mathrm{d}}$, $\ddot{\gamma}_{\mathrm{d}}$, and $\dddot{\gamma}_{\mathrm{d}}$.

4. Stability Analysis

Theorem 7. *For the velocity subsystem of AHV (17), considering the saturation characteristic of Φ (11), and adopting the control law (26) and the adaptive law (37) under the premise of Theorem 1, the closed-loop control system is semiglobally uniformly ultimately bounded.*

Proof 6. Define the estimation error of ω_V

$$\tilde{\omega}_V = \widehat{\omega}_V - \omega_V. \tag{73}$$

Substitute (26), (27), (35), and (36) into (25)

$$\begin{aligned}
\dot{\tilde{V}} &= \Phi_0^* - \Phi_1^* + F_V^*(V,\Phi^*) - \dot{V}_{\mathrm{ref}}\\
&= -k_{V1}\tilde{V} - k_{V2}\int_0^t \tilde{V}d\tau - \frac{1}{2}\tilde{V}\widehat{\omega}_V\mathbf{h}^{\mathrm{T}}(\mathbf{X}_1)\mathbf{h}(\mathbf{X}_1)\\
&\qquad + \mathbf{W}_V^{*\mathrm{T}}\mathbf{h}(\mathbf{X}_1) + \varepsilon.
\end{aligned} \tag{74}$$

Choose the following Lyapunov function candidate:

$$L_V = \frac{\tilde{V}^2}{2} + \frac{k_{V2}}{2}\left(\int_0^t \tilde{V}d\tau\right)^2 + \frac{\tilde{\omega}_V^2}{2\mu_V}. \tag{75}$$

Taking time derivative of (75) and invoking (37), (73) and (74) yield

$$\begin{aligned}
\dot{L}_V &= \tilde{V}\dot{\tilde{V}} + k_{V2}\tilde{V}\int_0^t \tilde{V}d\tau + \frac{\tilde{\omega}_V\dot{\widehat{\omega}}_V}{\mu_V}\\
&= \tilde{V}\left[-k_{V1}\tilde{V} - k_{V2}\int_0^t \tilde{V}d\tau - \frac{1}{2}\tilde{V}\widehat{\omega}_V\mathbf{h}^{\mathrm{T}}(\mathbf{X}_1)\mathbf{h}(\mathbf{X}_1) + \mathbf{W}_V^{*\mathrm{T}}\mathbf{h}(\mathbf{X}_1) + \varepsilon\right]\\
&\quad + k_{V2}\tilde{V}\int_0^t \tilde{V}d\tau + \frac{\tilde{\omega}_V}{\mu_V}\left(\frac{\mu_V}{2}\tilde{V}^2\mathbf{h}^{\mathrm{T}}(\mathbf{X}_1)\mathbf{h}(\mathbf{X}_1) - 2\widehat{\omega}_V\right)\\
&= -k_{V1}\tilde{V}^2 - \frac{1}{2}\tilde{V}^2\omega_V\mathbf{h}^{\mathrm{T}}(\mathbf{X}_1)\mathbf{h}(\mathbf{X}_1) + \tilde{V}\mathbf{W}_V^{*\mathrm{T}}\mathbf{h}(\mathbf{X}_1) + \tilde{V}\varepsilon - \frac{2\tilde{\omega}_V\widehat{\omega}_V}{\mu_V}.
\end{aligned} \tag{76}$$

Notice that

$$\begin{aligned}
\tilde{V}\mathbf{W}_V^{*\mathrm{T}}\mathbf{h}(\mathbf{X}_1) &\le \frac{\tilde{V}^2}{2}\left\|\mathbf{W}_V^{*\mathrm{T}}\mathbf{h}(\mathbf{X}_1)\right\|^2 + \frac{1}{2},\\
\tilde{V}\varepsilon &\le \frac{\tilde{V}^2}{4} + \varepsilon_M^2,\ 2\tilde{\omega}_V\widehat{\omega}_V \ge \tilde{\omega}_V^2 - \omega_V^2.
\end{aligned} \tag{77}$$

Also from Cauchy-Schwarz inequality

$$\left\|\mathbf{W}_V^{*\mathrm{T}}\mathbf{h}(\mathbf{X}_1)\right\| \le \|\mathbf{W}_V^*\|\|\mathbf{h}(\mathbf{X}_1)\|. \tag{78}$$

Further,

$$\begin{aligned}
\tilde{V}\mathbf{W}_V^{*\mathrm{T}}\mathbf{h}(\mathbf{X}_1) &\le \frac{\tilde{V}^2}{2}\|\mathbf{W}_V^*\|^2\|\mathbf{h}(\mathbf{X}_1)\|^2 + \frac{1}{2}\\
&= \frac{\tilde{V}^2}{2}\omega_V\mathbf{h}^{\mathrm{T}}(\mathbf{X}_1)\mathbf{h}(\mathbf{X}_1) + \frac{1}{2}.
\end{aligned} \tag{79}$$

Then (76) becomes

$$\dot{L}_V \le -\left(k_{V1} - \frac{1}{4}\right)\tilde{V}^2 - \frac{\tilde{\omega}_V^2}{\mu_V} + \frac{1}{2} + \varepsilon_M^2 + \frac{\omega_V^2}{\mu_V}. \tag{80}$$

Let $k_{V1} > 1/4$, and define the following compact sets:

$$\Omega_{\tilde{V}} = \left\{ \tilde{V} \mid \left|\tilde{V}\right| \le \sqrt{\frac{(1/2) + \varepsilon_M^2 + \left(\omega_V^2/\mu_V\right)}{(k_{V1} - (1/4))}} \right\},$$
$$\Omega_{\tilde{\omega}_V} = \left\{ \tilde{\omega}_V \mid |\tilde{\omega}_V| \le \sqrt{\frac{(1/2) + \varepsilon_M^2 + \left(\omega_V^2/\mu_V\right)}{(1/\mu_V)}} \right\}. \tag{81}$$

If $\tilde{V} \notin \Omega_{\tilde{V}}$ or $\tilde{\omega}_V \notin \Omega_{\tilde{\omega}_V}$, then $\dot{L}_V < 0$. Therefore, the closed-loop control system is semiglobally uniformly ultimately bounded. Further, these error signals $\tilde{V}$ and $\tilde{\omega}_V$ are semiglobally uniformly ultimately bounded and can be invariant to the following sets $\Omega_{\tilde{V}}$ and $\Omega_{\tilde{\omega}_V}$. The radiuses of $\Omega_{\tilde{V}}$ and $\Omega_{\tilde{\omega}_V}$ can be made arbitrarily small by choosing k_{V1} that is big enough and μ_V that is small enough, and the tracking errors $\tilde{V}$ and $\tilde{\omega}_V$ can also be arbitrarily small.

Theorem 8. *For the altitude subsystem of AHV (51), considering the saturation characteristic of δ_e (11) and adopting the control law (59), the adaptive law (69) and FD (72) under the premise of Theorem 4, the closed-loop control system is semiglobally uniformly ultimately bounded.*

Proof 7. Define the estimation error of ω_h

$$\tilde{\omega}_h = \hat{\omega}_h - \omega_h. \tag{82}$$

Then, define the estimation error of FD

$$\begin{aligned} \chi_1 &= \hat{z}_2 - z_2, \\ \chi_2 &= \hat{z}_3 - z_3, \\ \chi_3 &= \dot{\hat{\gamma}}_d - \dot{\gamma}_d, \\ \chi_4 &= \ddot{\hat{\gamma}}_d - \ddot{\gamma}_d, \\ \chi_5 &= \dddot{\hat{\gamma}}_d - \dddot{\gamma}_d. \end{aligned} \tag{83}$$

According to Theorem 6, there is $\chi_{iM} \in \mathbf{R}^+$ $(i = 1, 2, \ldots, 5)$

$$\chi_i \le \chi_{iM}. \tag{84}$$

Substitute (59), (67), and (68) into (58)

$$\dot{\hat{E}} = -k_{h1}\hat{E} - \frac{1}{2}\hat{E}\hat{\omega}_h \mathbf{h}^{\mathrm{T}}(\mathbf{X}_2)\mathbf{h}(\mathbf{X}_2) + \mathbf{W}_h^{*\mathrm{T}}\mathbf{h}(\mathbf{X}_2) + \iota. \tag{85}$$

Choose the following Lyapunov function candidate:

$$L_h = \frac{1}{2}\hat{E}^2 + \frac{\tilde{\omega}_h^2}{2\mu_h}. \tag{86}$$

Taking time derivative of (86) and invoke (69), (82), and (85) yield

$$\begin{aligned} \dot{L}_h &= \hat{E}\dot{\hat{E}} + \frac{\tilde{\omega}_h \dot{\hat{\omega}}_h}{\mu_h} \\ &= \hat{E}\left[-k_{h1}\hat{E} - \frac{1}{2}\hat{E}\hat{\omega}_h \mathbf{h}^{\mathrm{T}}(\mathbf{X}_2)\mathbf{h}(\mathbf{X}_2) + \mathbf{W}_h^{*\mathrm{T}}\mathbf{h}(\mathbf{X}_2) + \iota\right] \\ &\quad + \frac{\tilde{\omega}_h}{\mu_h}\left[\frac{\mu_h}{2}\hat{E}^2 \mathbf{h}^{\mathrm{T}}(\mathbf{X}_2)\mathbf{h}(\mathbf{X}_2) - 2\hat{\omega}_h\right] \\ &= -k_{h1}\hat{E}^2 - \frac{1}{2}\hat{E}^2\omega_h \mathbf{h}^{\mathrm{T}}(\mathbf{X}_2)\mathbf{h}(\mathbf{X}_2) + \hat{E}\mathbf{W}_h^{*\mathrm{T}}\mathbf{h}(\mathbf{X}_2) \\ &\quad + \hat{E}\iota - \frac{2\tilde{\omega}_h\hat{\omega}_h}{\mu_h}. \end{aligned} \tag{87}$$

Since

$$\begin{aligned} \hat{E}\mathbf{W}_h^{*\mathrm{T}}\mathbf{h}(\mathbf{X}_2) &\le \frac{\hat{E}^2}{2}\left\|\mathbf{W}_h^{*\mathrm{T}}\mathbf{h}(\mathbf{X}_2)\right\|^2 + \frac{1}{2}, \\ \frac{2\tilde{\omega}_h\hat{\omega}_h}{\mu_h} &\ge \frac{\tilde{\omega}_h^2}{\mu_h} - \frac{\omega_h^2}{\mu_h}, \\ \hat{E}\iota \le \left|\hat{E}\iota\right| &\le \frac{\hat{E}^2}{4} + \iota_{\mathrm{M}}^2. \end{aligned} \tag{88}$$

According to Cauchy-Schwarz inequality,

$$\left\|\mathbf{W}_h^{*\mathrm{T}}\mathbf{h}(\mathbf{X}_2)\right\| \le \|\mathbf{W}_h^*\|\|\mathbf{h}(\mathbf{X}_2)\|. \tag{89}$$

Further,

$$\begin{aligned} \hat{E}\mathbf{W}_h^{*\mathrm{T}}\mathbf{h}(\mathbf{X}_2) &\le \frac{\hat{E}^2}{2}\|\mathbf{W}_h^*\|^2\|\mathbf{h}(\mathbf{X}_2)\|^2 + \frac{1}{2} \\ &= \frac{\hat{E}^2}{2}\omega_h \mathbf{h}^{\mathrm{T}}(\mathbf{X}_2)\mathbf{h}(\mathbf{X}_2) + \frac{1}{2}. \end{aligned} \tag{90}$$

Then (87) becomes

$$\dot{L}_h \le -\left(k_{h1} - \frac{1}{4}\right)\hat{E}^2 - \frac{\tilde{\omega}_h^2}{\mu_h} + \frac{1}{2} + \iota_{\mathrm{M}}^2 + \frac{\omega_h^2}{\mu_h}. \tag{91}$$

Let $k_{h1} > 1/4$, and define the following compact sets:

$$\Omega_{\hat{E}} = \left\{ \hat{E} \mid \left|\hat{E}\right| \le \sqrt{\frac{(1/2) + \iota_{\mathrm{M}}^2 + \left(\omega_h^2/\mu_h\right)}{k_{h1} - (1/4)}} \right\},$$
$$\Omega_{\tilde{\omega}_h} = \left\{ \tilde{\omega}_h \mid |\tilde{\omega}_h| \le \sqrt{\frac{(1/2) + \iota_{\mathrm{M}}^2 + \left(\omega_h^2/\mu_h\right)}{1/\mu_h}} \right\}. \tag{92}$$

If $\hat{E} \notin \Omega_{\hat{E}}$ or $\tilde{\omega}_h \notin \Omega_{\tilde{\omega}_h}$, then $\dot{L}_h < 0$. Thus, these error signals $\hat{E}$ and $\tilde{\omega}_h$ are semiglobally uniformly ultimately bounded and can be invariant to the following sets $\Omega_{\hat{E}}$ and $\Omega_{\tilde{\omega}_h}$. The radiuses of $\Omega_{\hat{E}}$ and $\Omega_{\tilde{\omega}_h}$ can be made arbitrarily

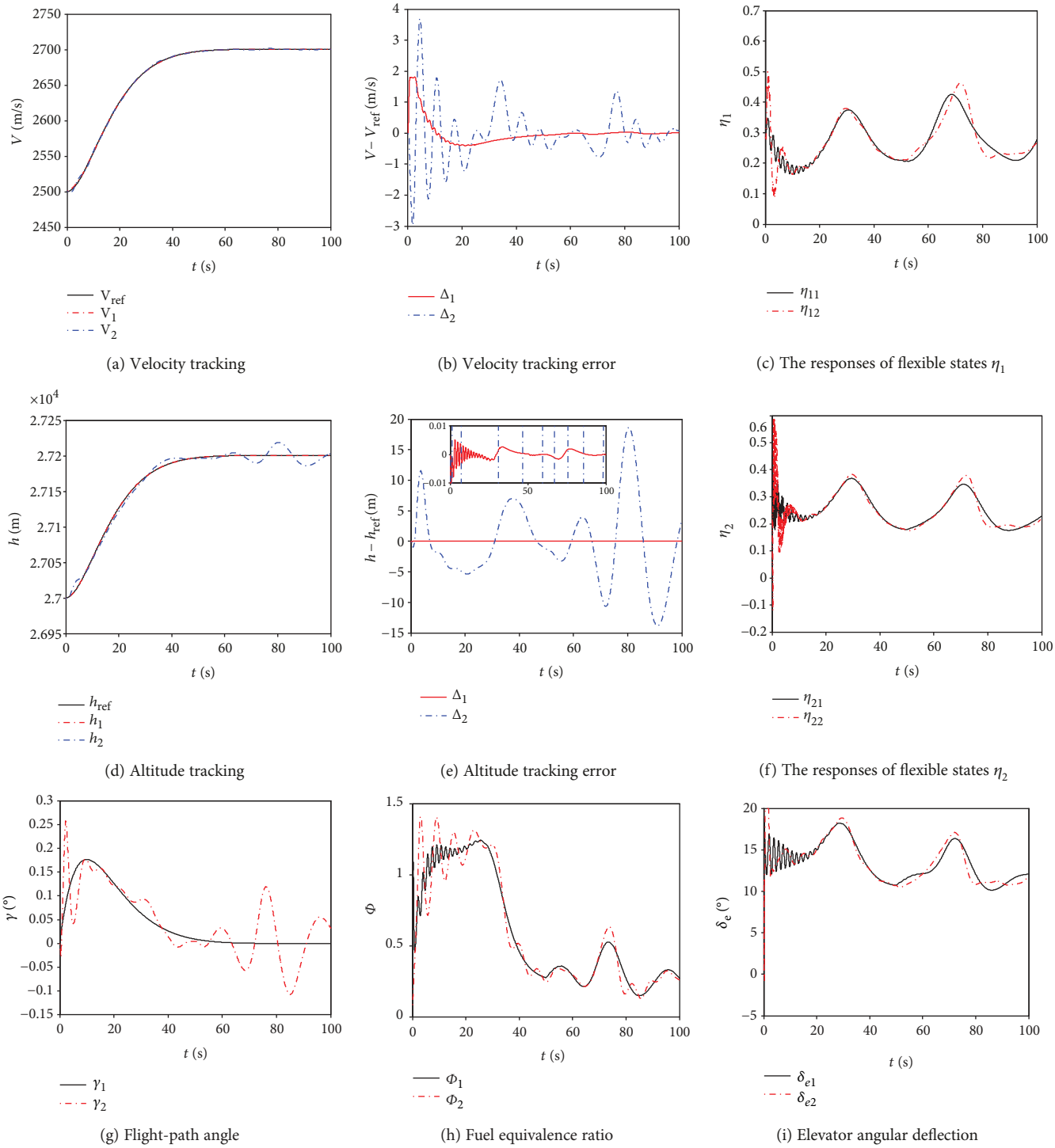

(a) Velocity tracking (b) Velocity tracking error (c) The responses of flexible states η_1

(d) Altitude tracking (e) Altitude tracking error (f) The responses of flexible states η_2

(g) Flight-path angle (h) Fuel equivalence ratio (i) Elevator angular deflection

FIGURE 2: Simulation result of Case 1.

small by choosing big enough k_{h1} and small enough μ_h, and the tracking errors $\widehat{E}$ and $\tilde{\omega}_h$ can also be arbitrarily small.

Combine (53), (54), (55) and (56) and (83)

$$E = \widehat{E} + \left(z_3 - \widehat{z}_3 + \ddot{\widehat{\gamma}}_d - \ddot{\gamma}_d\right) + 3\lambda\left(z_2 - \widehat{z}_2 + \dot{\widehat{\gamma}}_d - \dot{\gamma}_d\right) = \widehat{E} + \chi_4 - \chi_2 + 3\lambda(\chi_3 - \chi_1). \quad (93)$$

Consider (84), then (93) can become

$$E \le \widehat{E} + \chi_{4M} + \chi_{2M} + 3\lambda(\chi_{3M} + \chi_{1M}). \quad (94)$$

Therefore, E and e are also bounded, then the closed-loop control system is semiglobally uniformly ultimately bounded.

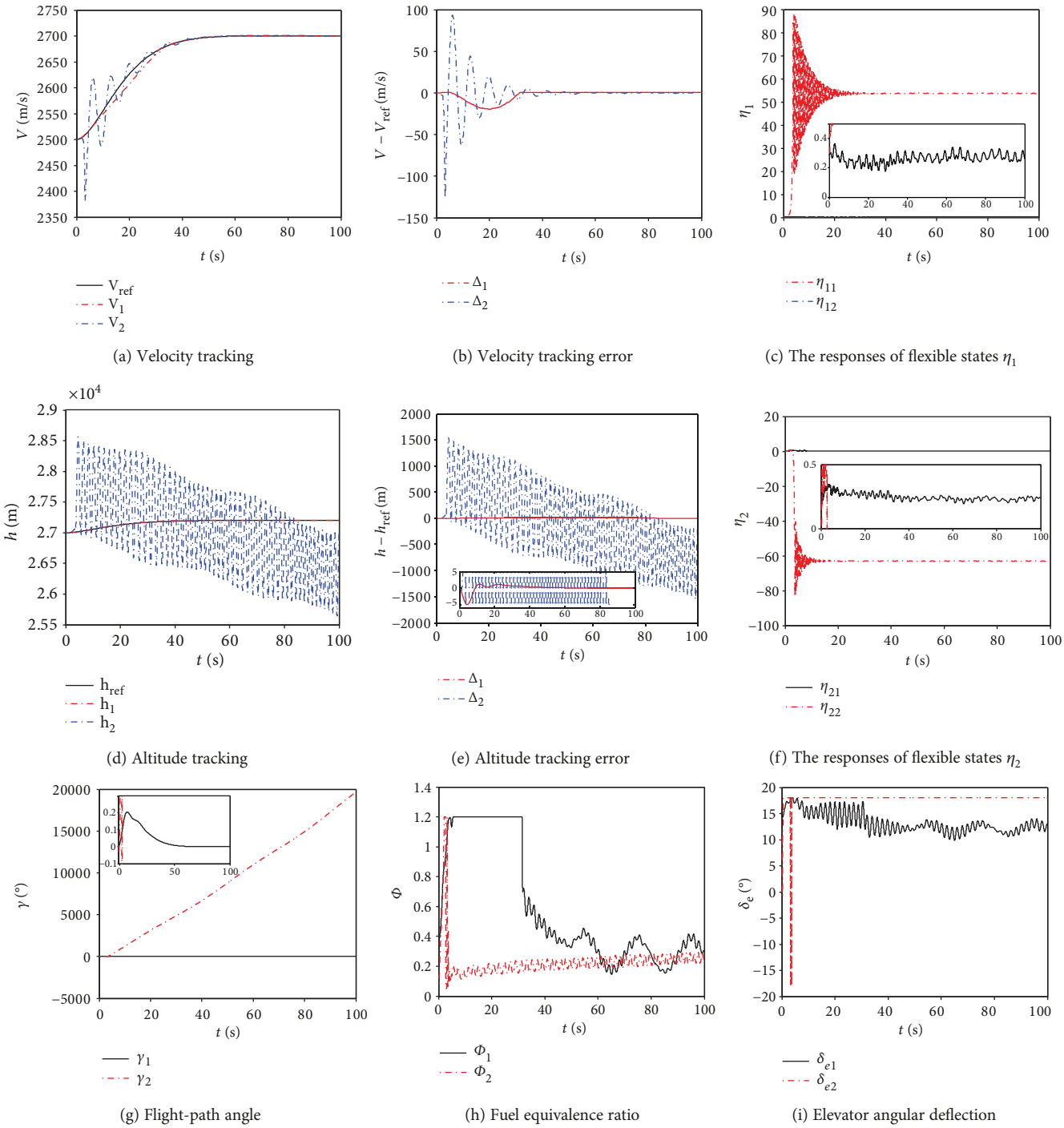

FIGURE 3: Simulation result of Case 2.

5. Simulation Results

With AHV longitudinal motion model as the controlled object, the tracking simulation of velocity and altitude reference commands is performed. The initial velocity and altitude of AHV are taken as $V = 2500$ m/s and $h = 27000$ m. Velocity step and altitude step are chosen as $\Delta V = 200$ m/s and $\Delta h = 200$ m. Both the velocity and altitude reference inputs are given by a second-order reference model with a damping ratio of 0.9 and a natural frequency of 0.1 rad/s. The design parameters of the controller are chosen as $k_V = 5$, $k_{V1} = 8$, $k_{V2} = 0.01$, $k_{\gamma 1} = 2$, $k_{\gamma 2} = 0.01$, $k_h = 0.9$, $k_{h1} = 30$, and $\lambda = 7$. The design parameters of the adaptive law are taken as $\mu_V = \mu_h = 0.05$. The design parameters of FD are chosen as $R_1 = R_2 = 0.05$, $a_{11} = a_{13} = a_{21} = a_{23} = 0.5$, and $a_{12} = a_{14} = a_{22} = a_{24} = 0.1$. The node number of RBFNN is chosen as $N_1 = N_2 = 20$. In the velocity subsystem, the center $\mathbf{c}_1$ of the Gaussian function is evenly spaced in [2500 m/s,

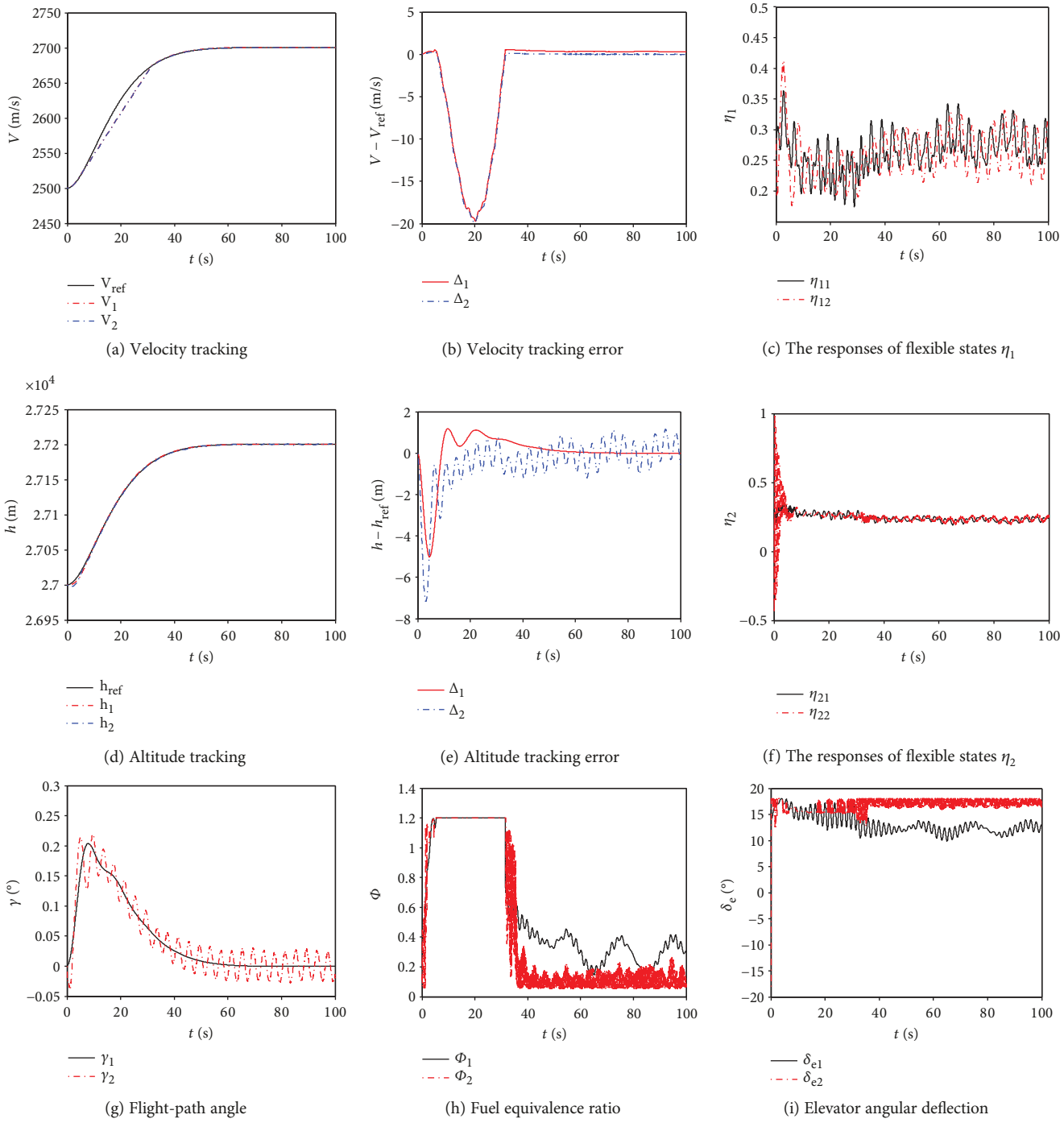

FIGURE 4: Simulation result of Case 3.

3100 m/s] × [−0.1, 1], and the width $\mathbf{b}_1$ is selected as 6.56. In altitude subsystem, the center $\mathbf{c}_2$ of the Gaussian function is evenly spaced in [−1°, 1°] × [0°, 5°] × [−5°/s, 5°/s] × [0 rad, 0.35 rad]; the width $\mathbf{b}_2$ is selected as 0.01. Three cases are considered in the simulation study.

Remark 9. In the above stability analysis of the control law, in order to ensure the stability of the closed-loop control system, the range of values of related parameters (such as $k_{V1} > 1/4$, $k_{h1} > 1/4$) is given. At the same time, in order to ensure tracking accuracy, the selection principle of related parameters is also analyzed (e.g., parameters k_{V1} and k_{h1} should be taken large enough, and parameters μ_V and μ_h should be taken small enough). The selection of parameters in the simulation is based on the above principles and is determined by repeated debugging.

Case 1. Considering Remark 1, we assume that actuators are constrained as $\Phi \in [0.05, 1.5]$ and $\delta_e \in [-20°, 20°]$. Simultaneously, to verify the robustness of the controller, it is

assumed that there is a perturbation of ±40% for the aerodynamic coefficient of the AHV model, which is expressed as $C = C_0[1 + 0.4 \sin(0.1\pi t)]$, where C_0 represents the nominal value and C stands for the simulation value. And after 50 s, add external disturbances $d_1 = 2 \sin(0.1\pi t)$ and $d_2 = 0.02 \sin(0.1\pi t)$ to (1) and (5) in the AHV model, respectively. The subscript "1" in the figures shows the result obtained by the proposed method, and the subscript "2" shows the result obtained by the method of [27].

Case 2. Combining Remark 2, we further suppose that actuators are subject to stricter constraints, resulting in a smaller executable range than the theoretical value, which are taken as $\Phi \in [0.05, 1.2]$ and $\delta_e \in [-18^\circ, 18^\circ]$. Other simulation conditions are the same as Case 1.

Case 3. The control problem of nonlinear systems with actuator constraints has been considered extensively in the existing results, such as [28, 29]. In order to compare with the method in this paper, the adaptive dynamic surface control method considering actuator constraints proposed in [29] is applied to the AHV model. All conditions in the simulation are the same as in Case 2. The subscript "1" represents the result of the proposed method. The subscript "2" represents the result of the method proposed in [29].

When the control inputs are constrained as described in Case 1 (see Figures 2(h) and 2(i)), both the proposed method and method of [26] can guarantee that V and h track their reference commands V_{ref} and h_{ref} (see Figures 2(a) and 2(d)). However, the tracking accuracy and anti-interference ability of the proposed method in this paper are significantly improved than those of the method in [26] (see Figures 2(b) and 2(e)). At the same time, the changes in the flight-path angle and flexible states are also smoother than [26] (see Figures 2(c), 2(f), and 2(g)). When actuators of AHV are subject to stricter constraints (see Figures 3(h) and 3(i)), the stability of the closed-loop system cannot be guaranteed with the method of [26]. But through using the proposed method in this paper, the control objective can still be achieved (see Figures 3(a), 3(b), 3(d), and 3(e)). And the proposed method can effectively inhibit flexible states (see Figures 3(c) and 3(f)). In Case 3, the method proposed in [29] can guarantee that V and h track their reference commands when the actuators are constrained (see Figures 4(a) and 4(d)). However, since the method does not use the relevant means to estimate the uncertain dynamics of the model, the tracking error is significantly larger than the method proposed in this paper (see Figures 4(b) and 4(e)). At the same time, compared with the method in [29], the control curve obtained by the method is smoother (see Figures 4(h) and 4(i)), which is more suitable for engineering applications.

6. Conclusion

(1) An adaptive neural control law based on input saturation function is designed in this paper, which guarantees the stability of the closed-loop system and the boundedness of tracking error when the actuator reaches saturation.

(2) When the AHV model encounters perturbation of aerodynamic coefficient and external disturbances, the proposed method can still ensure good tracking accuracy, which proves that the algorithm has strong robustness.

(3) The controller designed in this paper can still effectively suppress the flexible states when the actuator is constrained. Simulation examples verify the effectiveness and superiority of the design method.

(4) In this paper, only the most common amplitude saturation problem of the actuator is considered, and the rate and bandwidth constraint problem is not discussed. These will serve as a further research direction.

Data Availability

The data used to support the findings of this study are included within the article.

Conflicts of Interest

The authors declare that they have no conflicts of interest.

Acknowledgments

This study was cosupported by the National Natural Science Foundation of China (Grant no. 61573374 and no. 61703421).

References

[1] E. A. Morelli, "Flight-test experiment design for characterizing stability and control of hypersonic vehicles," *Journal of Guidance, Control, and Dynamics*, vol. 32, no. 3, pp. 949–959, 2009.

[2] D. Preller and M. K. Smart, "Longitudinal control strategy for hypersonic accelerating vehicles," *Journal of Spacecraft and Rockets*, vol. 52, no. 3, pp. 993–999, 2015.

[3] L. G. Wu, H. An, J. X. Liu, and C. H. Wang, "Recent progress in control of air-breathing hypersonic vehicles," *Journal of Harbin Institute of Technology*, vol. 48, no. 10, pp. 1–16, 2016.

[4] H. B. Duan and P. Li, "Progress in control approaches for hypersonic vehicle," *Science China Technological Sciences*, vol. 55, no. 10, pp. 2965–2970, 2012.

[5] B. Xu and Z. K. Shi, "An overview on flight dynamics and control approaches for hypersonic vehicles," *Science China Information Sciences*, vol. 58, no. 7, pp. 1–19, 2015.

[6] F. Yang, R. Yuan, J. Yi, G. Fan, and X. Tan, "Direct adaptive type-2 fuzzy neural network control for a generic hypersonic flight vehicle," *Soft Computing*, vol. 17, no. 11, pp. 2053–2064, 2013.

[7] B. Xu, D. X. Gao, and S. X. Wang, "Adaptive neural control based on HGO for hypersonic flight vehicles," *Science China Information Sciences*, vol. 54, no. 3, pp. 511–520, 2011.

[8] B. Xu, D. Wang, F. Sun, and Z. Shi, "Direct neural discrete control of hypersonic flight vehicle," *Nonlinear Dynamics*, vol. 70, no. 1, pp. 269–278, 2012.

[9] X. Bu, X. Wu, Z. Ma, and R. Zhang, "Nonsingular direct neural control of air-breathing hypersonic vehicle via back-stepping," *Neurocomputing*, vol. 153, pp. 164–173, 2015.

[10] X. Bu, X. Wu, J. Huang, Z. Ma, and R. Zhang, "Minimal-learning-parameter based simplified adaptive neural back-stepping control of flexible air-breathing hypersonic vehicles without virtual controllers," *Neurocomputing*, vol. 175, Part A, pp. 816–825, 2016.

[11] X. Bu, X. Wu, R. Zhang, Z. Ma, and J. Huang, "A neural approximation-based novel back-stepping control scheme for air-breathing hypersonic vehicles with uncertain parameters," *Proceedings of the Institution of Mechanical Engineers, Part I: Journal of Systems and Control Engineering*, vol. 230, no. 3, pp. 231–243, 2016.

[12] C. Y. Sun, C. X. Mu, and Y. Yu, "Some control problems for near space hypersonic vehicles," *Acta Automatica Sinica*, vol. 39, no. 11, pp. 1901–1913, 2013.

[13] J. Li and B. Zuo, "Adaptive terminal sliding mode control for air-breathing hypersonic vehicles under control input constraints," *Acta Aeronautica et Astronautica Sinca*, vol. 33, no. 2, pp. 220–233, 2012.

[14] B. Xu, Z. Shi, C. Yang, and S. Wang, "Neural control of hypersonic flight vehicle model via time-scale decomposition with throttle setting constraint," *Nonlinear Dynamics*, vol. 73, no. 3, pp. 1849–1861, 2013.

[15] B. Xu, X. Huang, D. Wang, and F. Sun, "Dynamic surface control of constrained hypersonic flight models with parameter estimation and actuator compensation," *Asian Journal of Control*, vol. 16, no. 1, pp. 162–174, 2014.

[16] M. A. Bolender and D. B. Doman, "Nonlinear longitudinal dynamical model of an air-breathing hypersonic vehicle," *Journal of Spacecraft and Rockets*, vol. 44, no. 2, pp. 374–387, 2007.

[17] J. T. Parker, A. Serrani, S. Yurkovich, M. A. Bolender, and D. B. Doman, "Control-oriented modeling of an air-breathing hypersonic vehicle," *Journal of Guidance, Control, and Dynamics*, vol. 30, no. 3, pp. 856–869, 2007.

[18] X. Bu, X. Wu, Z. Ma, R. Zhang, and J. Huang, "Novel auxiliary error compensation design for the adaptive neural control of a constrained flexible air-breathing hypersonic vehicle," *Neurocomputing*, vol. 171, pp. 313–324, 2016.

[19] L. Fiorentini and A. Serrani, "Adaptive restricted trajectory tracking for a non-minimum phase hypersonic vehicle model," *Automatica*, vol. 48, no. 7, pp. 1248–1261, 2012.

[20] L. Fiorentini, *Nonlinear Adaptive Controller Design for Air-Breathing Hypersonic Vehicles*, The Ohio State University, Columbus, 2010.

[21] R. M. Sanner and J.-J. E. Slotine, "Gaussian networks for direct adaptive control," *IEEE Transactions on Neural Networks*, vol. 3, no. 6, pp. 837–863, 1992.

[22] A. J. Calise, N. Hovakimyan, and M. Idan, "Adaptive output feedback control of nonlinear systems using neural networks," *Automatica*, vol. 37, no. 8, pp. 1201–1211, 2001.

[23] J. H. Park, S. H. Huh, S. H. Kim, S. J. Seo, and G. T. Park, "Direct adaptive controller for nonaffine nonlinear systems using self-structuring neural networks," *IEEE Transactions on Neural Networks*, vol. 16, no. 2, pp. 414–422, 2005.

[24] S. S. Ge and C. Wang, "Adaptive NN control of uncertain nonlinear pure-feedback systems," *Automatica*, vol. 38, no. 4, pp. 671–682, 2002.

[25] X. Bu, "Guaranteeing prescribed output tracking performance for air-breathing hypersonic vehicles via non-affine back-stepping control design," *Nonlinear Dynamics*, vol. 91, no. 1, pp. 525–538, 2018.

[26] X. Wang, Z. Chen, and G. Yang, "Finite-time-convergent differentiator based on singular perturbation technique," *IEEE Transactions on Automatic Control*, vol. 52, no. 9, pp. 1731–1737, 2007.

[27] X. Bu, X. Wu, R. Zhang, Z. Ma, and J. Huang, "Tracking differentiator design for the robust backstepping control of a flexible air-breathing hypersonic vehicle," *Journal of the Franklin Institute*, vol. 352, no. 4, pp. 1739–1765, 2015.

[28] H. Wang, B. Chen, X. Liu, K. Liu, and C. Lin, "Robust adaptive fuzzy tracking control for pure-feedback stochastic nonlinear systems with input constraints," *IEEE Transactions on Cybernetics*, vol. 43, no. 6, pp. 2093–2104, 2013.

[29] L. Chen and Q. Wang, "Adaptive dynamic surface control for unknown pure feedback non-affine systems with multiple constraints," *Nonlinear Dynamics*, vol. 90, no. 2, pp. 1191–1207, 2017.